SCIENCE CHINA Materials ARTICLES

mater.scichina.com link.springer.com

Epitaxial thin-film $Pd_{1-x}Fe_x$ alloy – a tunable ferromagnet for superconducting spintronics

Alireza Esmaeili[1], Igor V. Yanilkin[1], Amir I. Gumarov[1], Iskander R. Vakhitov[1], Bulat F. Gabbasov[1], Roman V. Yusupov[1]*, Dmitriy A. Tatarsky[2], Lenar R. Tagirov[1,3]

ABSTRACT Thin epitaxial films of the palladium-rich $Pd_{1-x}Fe_x$ alloy were synthesized and extensively studied as a tunable ferromagnetic material for superconducting spintronics applications. The (001)-oriented MgO single-crystal substrate and the composition range of x = 0.01 - 0.07 were chosen to support epitaxial growth and provide the films with the magnetic properties spanning from magnetically very soft ferromagnet for memory applications to intermediately soft and moderately hard for the programmable logic and circuit biasing, respectively. Dependences of the saturation magnetization, Curie temperature and three magnetic anisotropy constants on the iron content x were obtained for the first time from the analysis of the magnetometry and ferromagnetic resonance data. The experimental results are discussed in the framework of existing theories of dilute ferromagnetic alloys. Simulation of the hysteresis loops within the Stoner-Wohlfarth model indicates the predominant coherent magnetic moment rotation at cryogenic temperatures. The obtained results compile a database of magnetic properties of a palladium-iron alloy in a single-crystal thin-film form considered as a material for superconducting spintronics.

Keywords: palladium-iron alloy, thin epitaxial films, magnetization, magnetic anisotropy, superconducting spintronics

INTRODUCTION

Conventional complementary metal–oxide–semiconductor (CMOS)-based electronics is already approaching its physical limits (see, for example, References [1-5] and citations therein) so the end of conventional Moore's law scaling [6] is really near. Approaches beyond the Moore suggest various solutions comprising new materials and devices, more efficient architectures and packaging, and new models of calculations [4,5]. One of them pushes forward heterogeneous multi-chip architectures/packages where every kind of calculations is performed by a specialized processor based on optimal device physics.

Forefront in the high-end supercomputing is associated now with superconducting Josephson-junction technology [7-10], which offers up to two orders increase in the clock frequency (100 GHz and beyond) and six orders reduction in the energy dissipation per bit operation – incredible gain against present semiconductor processors [11,12]. Requirement of the cryogenic cooling may seem a complication, which, however, should not scare thanks to the development of close-cycle refrigeration. The superconducting single flux quantum (SFQ) Josephson logic technology [13], was implemented in the US Cryogenic Computing Complexity (C3) Program [14,15], aiming to demonstrate a route towards the supercomputing system with the total performance of up to 1000 Pflops and utilizing sub-ns access time Josephson magnetic random access memory (MRAM) [16-18].

Josephson junctions incorporating ferromagnetic layers were proposed not only for the superconducting spintronic memory, but for the programmable and reconfigurable digital circuits, dissipationless and reconfigurable clock and biasing networks in SFQ circuits. To realize these applications, a ferromagnetic material which is weak in the sense of small spin-polarization of the conduction band is required [19,20], providing insensitivity to the interface roughness and the 10-30 nm range of the layer thickness comfortable for the deposition techniques. To restrict a number of materials involved into the production technology a tunable ferromagnet would be desired since clocking and biasing networks require non-switchable, magnetically hard ferromagnetic layer, while memory and reconfigurable logic involve soft ferromagnets with low but different switching fields. Robustness of the magnetic properties is another important requirement to a material for commercial electronic devices. The $Pd_{1-x}Fe_x$ alloy with x = 0.01-0.03 was considered as material of a choice for a weak and soft ferromagnet in superconducting MRAM [16,21-23]. Nevertheless, no further development towards a prototype has been demonstrated utilizing the $Pd_{1-x}Fe_x$ alloy. Instead, the Josephson magnetic memory cell con-

[1] Institute of Physics, Kazan Federal University, Kazan 420008, Russia
[2] Institute for Physics of Microstructures of RAS, Nizhny Novgorod 603950, Russia
[3] Zavoisky Physical-Technical Institute, FRC Kazan Scientific Center of RAS, Kazan 420029, Russia
* Corresponding author (Roman.Yusupov@kpfu.ru)

trolled by a pseudo-spin-valve was demonstrated using a combination of Ni and Py (permalloy), the latter serving as a soft switchable component in the nanometer-thickness range [24].

Tunability of magnetism in the palladium-rich $Pd_{1-x}Fe_x$ alloy was extensively studied for the bulk [25]. Much less information is available on the properties of palladium-iron films. In particular, predominantly the polycrystalline films with low iron content ($x \sim 0.01$) have been investigated [26-30]. We could find only few reports on studies of thin Pd-rich alloy films grown with MBE technique, albeit no evidence of the epitaxial film growth had been given there [31-34]. The principal characteristics that determine an applicability of $Pd_{1-x}Fe_x$ alloys for thin-layer superconductor/ferromagnet/superconductor (S/F/S) type Josephson structures are the saturation magnetization (controls the conduction band exchange splitting) and magnetic anisotropy (determines coercivity and, hence, the switching fields). In this paper we present a systematic study of the magnetic properties variation with the composition of palladium-rich $Pd_{1-x}Fe_x$ ($x = 0.01$-0.07) alloy thin films epitaxially grown on the single-crystal MgO(001) substrate, targeting at a low-temperature weak and tunable ferromagnet suitable for superconducting spintronics.

EXPERIMENTAL SECTION

Methods and samples

Epitaxial films of $Pd_{1-x}Fe_x$ ($x = 0.011 - 0.07$) alloy with the thickness of 20 nm were grown on epi-polished (100)-oriented MgO substrates (*MTI Corp., USA*) utilizing molecular beam epitaxy (MBE) technique in the ultra-high vacuum (UHV) chamber (*SPECS GmbH, Germany*). The pressure during the depositions was in the range of $(3–5)\times10^{-10}$ mbar. The metallic Fe and Pd pellets were simultaneously co-evaporated from pre-calibrated high-temperature effusion cells (*CreaTec Fischer & Co., Germany*). Three-step deposition procedure [35] was applied to obtain 20 nm thick, smooth and compositionally homogeneous epitaxial films of $Pd_{1-x}Fe_x$ ($x < 0.10$) alloy [36]. The representative transmission electron microscopy (TEM) image, and the selected-area electron diffraction pattern (SAED) from the $MgO/Pd_{1-x}Fe_x$ interface (**Figure 1**) confirm epitaxial "cube-on-cube" growth mode of the palladium-iron alloy film on the single-crystalline MgO(100) substrate. More details of the samples preparation and characterization routines can be found in Ref. [36].

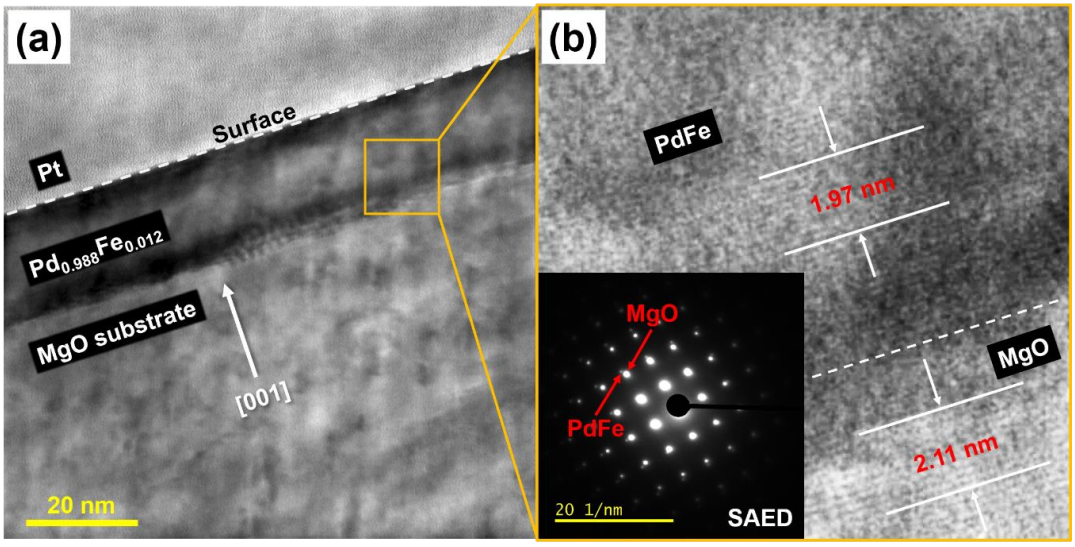

Figure 1 (a) TEM image of the sample cross-section; (b) magnified area of the $Pd_{0.988}Fe_{0.012}$/MgO(001) interface where ten interplanar distances are marked for both materials. The inset shows the selected area electron diffraction (SAED) pattern taken from the interface. High quality of the contrast, reflecting the cubic symmetry of the lattice, is an indication of the single-crystal character of the interface area. Two sets of the superimposed diffraction spots correspond to the MgO lattice (smaller pitch size is due to the larger lattice parameter $a_{MgO} = 421.6$ pm) and $Pd_{0.989}Fe_{0.011}$ lattice (larger pitch size, $a_{Pd} = 389.1$ pm).

Magnetic properties of the synthesized samples, which are of primary importance for the superconducting spintronic applications, were studied with the vibrating sample magnetometry (VSM, *Quantum Design PPMS-9 system*) and ferromagnetic resonance (FMR, *Bruker ESP300 cw X-band spectrometer*) techniques. The temperature dependences of the magnetic moment $M(T)$ were measured on sample warming from 5 K to 300 K at a rate of 3 K·min^{-1} in the saturating magnetic field of 30 Oe applied in the film plane ("in-plane" geometry) along the film easy axis. Magnetic hysteresis loops were recorded with the sweep rate of 2.3 Oe·sec^{-1}. The measured magnetic moment was reduced to the number of Bohr magnetons (μ_B) per iron atom as well as to the volume magnetization of the film (emu·cm^{-3}). The diamagnetic and paramagnetic contributions of the MgO substrate were subtracted from the collected VSM data. The FMR measurement geometries and interpretation routines are described in Ref. [37].

RESULTS

Figure 2a shows the temperature dependence of the saturation magnetization for a composition series of $Pd_{1-x}Fe_x$ films. In **Figure 2b**, the same set of the dependencies is presented in the reduced $M_s/M_s(0)$ vs T/T_C coordinates. Clearly, these temperature dependencies have practically identical shape for all studied concentrations of iron, though this common dependence is significantly different from that for the pure iron (also shown in Figure 2b). We will address this observation later, in the ANALYSIS AND DISCUSSION section.

As expected, both the film saturation magnetization M_s and the Curie temperature T_C raise monotonically with the increase of the iron content x (see **Table 1**). Maximum magnetic moment per iron atom of $M_{Fe} \simeq 7.5\ \mu_B$/Fe is found for the $x = 0.017$ sample. This is in a good agreement with the results for the bulk $Pd_{1-x}Fe_x$, where the values of $\simeq 10\ \mu_B$/Fe for $x = 0.01$ and $\simeq 5.5\ \mu_B$/Fe for $x = 0.1$ have been reported [39]. However, the obtained result is considerably larger than $\sim 3.7\ \mu_B$/Fe for a non-epitaxial $Pd_{0.99}Fe_{0.01}$ film [29].

Magnetic anisotropy of the films has been characterized utilizing the FMR technique. The FMR spectra were recorded at $T = 10$ K for the samples with $x = 0.011 - 0.019$ ($T_C < 100$ K), and at $T = 20$ K for the samples with higher iron content. **Figure 3a** shows representative angular dependences of the FMR resonance field for the in-plane geometry of the measurements (external magnetic field is rotated in the film plane). The samples reveal the four-fold in-plane magnetic anisotropy with the easy directions along the ⟨110⟩ axes, which is typical for single-crystalline materials. For instance, Bagguley *et al.* have reported that the bulk single-crystalline $Pd_{0.983}Fe_{0.017}$ alloy reveals the cubic anisotropy with the hard directions along the ⟨100⟩ axes [40]. The four-fold anisotropy with the easy ⟨110⟩ axes in the film plane was found also for nominally epitaxial $Pd_{1-x}Fe_x$ ($x \simeq 0.04$ and 0.10) films by Garifullin *et al.* [32].

Figure 3b shows hysteresis loops for three representative $Pd_{1-x}Fe_x$ films with different iron content. It is clear from the shape of the loops, as well as from the FMR angular dependences, that the anisotropy becomes stronger with an increase of the iron content x (see Figures 3a and 3b). Coercivity H_c also depends on the iron content and varies from 5.5 to 23 Oe (see Table 1). The observed coercive field values are consistent with those reported for polycrystalline films, compare with $H_c \simeq 5$ Oe for $x = 0.01$ [30] and $H_c \simeq 25$ Oe for $x = 0.072$ [34].

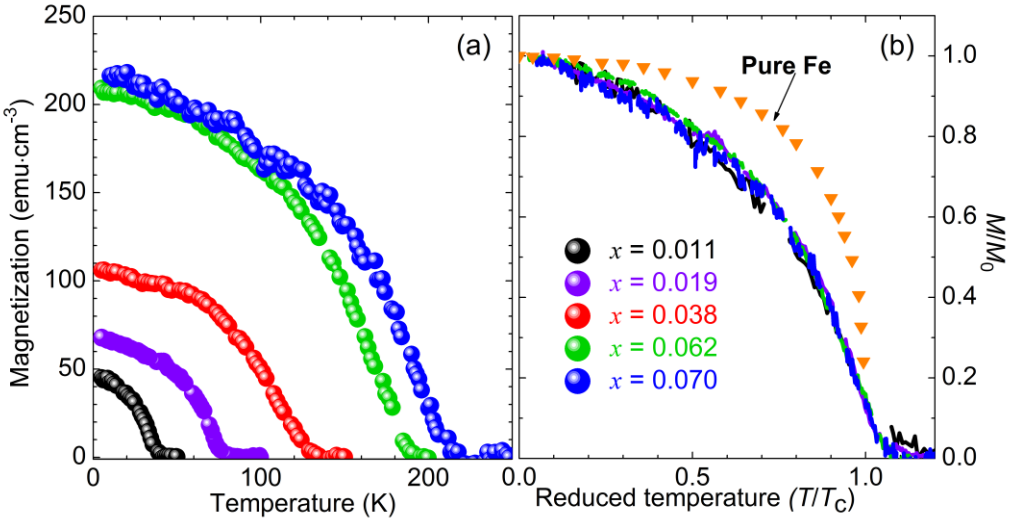

Figure 2 Temperature dependence of the saturation magnetization for a series of 20-nm thick epitaxial $Pd_{1-x}Fe_x$ films on MgO(001), in the absolute (a) and the reduced (b) coordinates. Normalized $M_s(T/T_C)/M_s(0)$ dependence for pure iron is given for a comparison (orange symbols, adopted from Reference [38]).

Table 1 Experimental parameters of epitaxial $Pd_{1-x}Fe_x$ alloy films with different iron content.

x, from XPS	T_C (K)	M_s (emu·cm^{-3})	[a] M_{Fe} (μ_B)	[b] H_c (Oe)		[c] g-factor
				easy	hard	
0.011±0.001	36±2	52±4	6.8±0.9	8.8±1.0	7.0±1.0	2.19
0.014±0.001	49±2	63±4	7.1±0.9	7.5±1.0	5.5±1.0	2.20
0.017±0.001	72±3	83±5	7.5±0.8	16.7±1.0	14.7±1.0	2.18
0.019±0.002	73±3	85±5	6.5±0.8	10.1±1.0	7.8±1.0	2.15
0.038±0.002	120±4	119±6	5.3±0.6	8.5±1.0	9.0±1.0	2.15
0.062±0.002	177±5	211±11	5.6±0.5	17.0±1.0	18.5±1.0	2.17
0.070±0.002	200±5	216±11	4.3±0.3	23.0±1.0	15.0±1.0	2.13

[a] Magnetic moment per iron atom; b) Coercive filed measured at 5 K along easy or hard axes of the film; c)For the g-factor, experimental uncertainties are less than 0.004 for all samples.

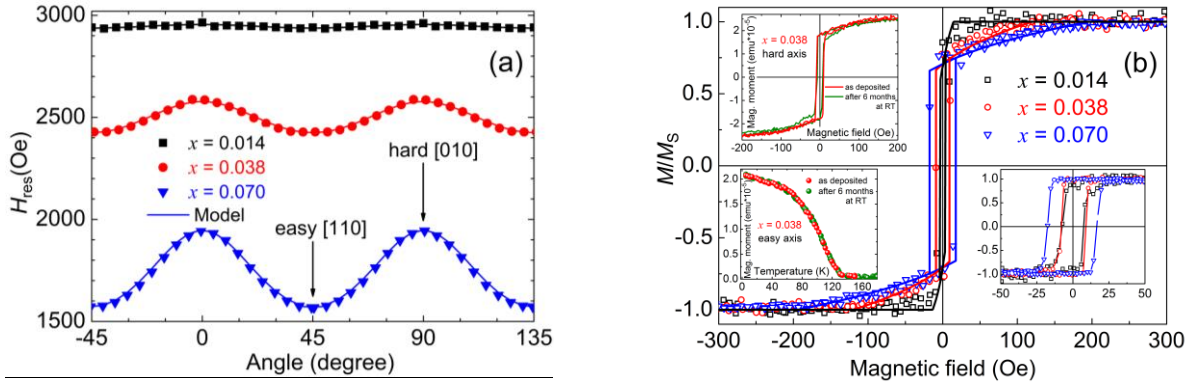

Figure 3 (a) Angular dependences of the FMR resonance field for the in-plane measurements of Pd1-xFex films with different iron content (symbols – experimental data, lines – fitting results); the measurement temperature T = 10 K for x = 0.014 sample and T = 20 K for x = 0.036 and x = 0.070; (b) In-plane magnetic hysteresis loops of Pd1-xFex alloy films measured at 5 K with the field applied along the hard [100] axis of the film. Right-bottom inset – the same along the easy [110] axis. Left-top and left-bottom insets demonstrate the long-term stability of the hysteretic and magnetization properties after 6 months at ambient conditions.

ANALYSIS AND DISCUSSION

To analyze the temperature dependence of the magnetic moment and the concentration dependence of the ferromagnetic transition temperature T_C, several theoretical models can be applied. These models utilize different approaches in their theoretical frameworks and provide physical parameters suitable for a comparative analysis.

Temperature dependence of the magnetic moment. Identification of the magnetism type

Spin-Fluctuation Model

The magnetic moment per iron atom in $Pd_{1-x}Fe_x$ series (Table 1) varies from 4.3 μ_B to 7.5 μ_B at saturation, while that in the metallic iron it is about 2.2 μ_B (see, for example, Ref. [41], Ch. 5, Table 5.1; and Ref. [42], Ch. 5, Table 5.4). This suggests a dominance of the palladium contribution to the total magnetic moment of $Pd_{1-x}Fe_x$ (x = 0.011 – 0.07) alloy (or almost equivalent contributions from the iron and the palladium in the case of the highest iron content, x = 0.07, with 4.3 μ_B per iron atom). The universal temperature dependence of the magnetic moment, Figure 2b, for different concentrations of iron in the studied range makes it reasonable to fit the $M_s(T)$ data within the most general approach, which takes into account the itineracy of electrons carrying magnetism. The approach is based on the Landau-type expansion in a power series in magnetization up to higher orders to account for spin fluctuations [41,43-46]. In the latest analysis by Kuz'min, an equation for the reduced magnetization $\sigma(T) = M_s(T)/M_s(0)$ is given, which can be used to fit the experimental $M_s(T)$ from Figure 2b [46]:

$$\sigma^2(\tau) = \frac{\sqrt{\kappa^2 + 4(1-\kappa)(1-\tau^3)\Big/(1+p\tau^{3/2})} - \kappa}{2(1-\kappa)}. \quad (1)$$

Here, $\tau = T/T_C$, and κ is a dimensionless ratio of the Landau expansion coefficients (of the fourth order to the second order), which depends on the relationship of

nonlinear and linear susceptibilities balanced by the saturation magnetization extrapolated to zero temperature [46]. The parameter p provides a correct low-temperature behavior of the magnetic moment $M_s(T)$ (for example, providing compliance with the Bloch-$T^{3/2}$ law for fixed-spin Heisenberg model with spin-wave excitations). The fit of the experimental data (**Figure 4a**) has given $p = -0.02 \pm 0.05$, $\kappa = 2.1 \pm 0.1$. This parameter set is in a drastic contrast with that of $p = 0.95 \pm 0.12$, and $\kappa = 0.86 \pm 0.07$, obtained for gadolinium, which is the localized-spin $S = 7/2$ ferromagnet [47]. Similar data for nickel, which is the iron-group ferromagnetic metal with much higher degree of delocalization of its *d*-electrons compared with *f*-electrons of gadolinium, has given $p = 0.28$ and $\kappa = 0.47$ which lie somewhere in between of $Pd_{1-x}Fe_x$ and gadolinium [46]. This observation provides a further evidence of a dominant itinerant carriers contribution to the spontaneous magnetization of $Pd_{1-x}Fe_x$ alloys in the range of $x = 0.01 - 0.07$.

Handrich-Kobe Model

Nanoscale composition inhomogeneity is a distinctive feature of alloys with respect to elementary metals or stoichiometric compounds. This also affects the shape of the magnetization dependence on temperature. Handrich-Kobe model uses a modified Brillouin function with the distribution of the exchange coupling strength in the positionally disordered environment [48,49]. The reduced magnetization is expressed as:

$$\sigma(\tau) = \frac{1}{2}\ B_S\left[\,1+\delta\ y\right] + B_S\left[\,1-\delta\ y\right]\,, \qquad (2)$$

where $y = \left[3S/(S+1)\right]\sigma(\tau)/\tau$, B_S – the conventional (spin-only) Brillouin function and S is the magnetic atom spin value. The exchange fluctuation parameter is defined as $\delta = \sqrt{\left\langle \Delta J^2 \right\rangle / \left\langle J \right\rangle^2}$, where J is the exchange integral.

Taking $S = 3/2$, as it follows from the closest proximity from the above to provide the magnetic moment value per atom $\mu(\mathrm{Fe}) = 2.2\ \mu_B$ in metallic iron, we obtain $\delta = 0.48$ from the fit of our experimental data (see Figure 4a). The sensitivity of the theory to the spin value appears to be weak: δ-value varies in the range of 0.45 – 0.53 when the spin S is varied from 5/2 to 1, respectively. The fluctuations of the exchange integral flatten the $M_s(T)$-dependence against the ideal compositional order ($\delta = 0$ for pure iron) (see Figure 4a). The value of $\delta \approx 0.48$ is close to that found for amorphous iron-containing ferromagnets, for instance, $\delta = 0.5$ for $Fe_{80}B_{12}Nb_8$ [47] and $\delta = 0.55$ for $Fe_{88}Zr_7B_4Cu_1$ [50]. Exchange fluctuation parameter δ originates from the compositional (structural) disorder and corresponding distribution of distances to the nearest magnetic neighbors. In this respect, $Pd_{1-x}Fe_x$ alloy with random arrangement of iron atoms is just another nonzero-δ case. Hence, the application of the Handrich-Kobe approach seems to be adequate, despite it completely ignores the contribution of the palladium constituent to the net moment of the alloy.

Korenblit-Shender-Shklovsky Model

A commonly accepted physical picture supposes that an iron atom embedded into paramagnetic palladium magnetizes electrons of the host matrix around it because of the *d*-electron hybridization (see, for example, Ref. [41], Ch. 15). Thus, it creates a local "bubble" of magnetized palladium atoms around. On cooling, the bubbles of spin-polarized palladium electrons grow in size, and at a temperature when they overlap, the long-range ferromagnetic order sets in. The onset of ferromagnetism thereby occurs through a percolation process involving these spin-polarized bubbles [51].

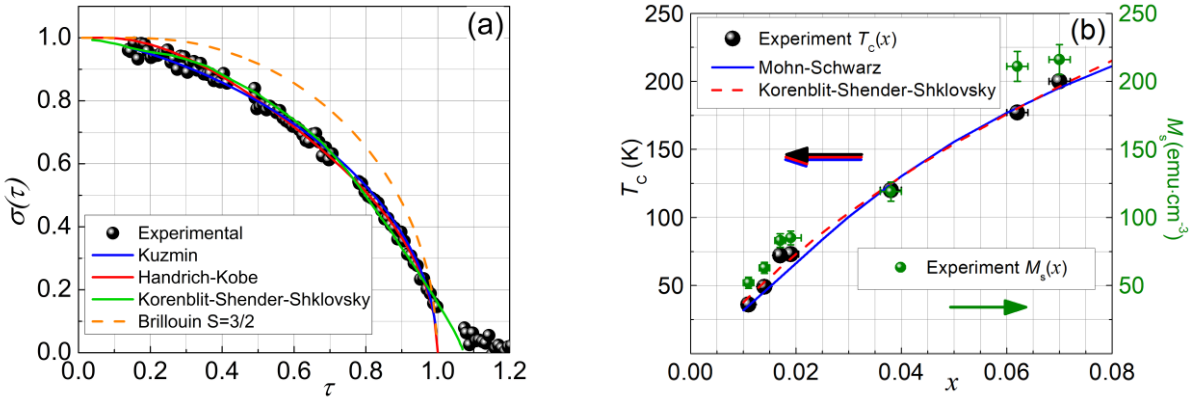

Figure 4 (a) Normalized saturation magnetization σ dependence on the reduced temperature τ of the $Pd_{0.989}Fe_{0.011}$ film (solid symbol) and its fits with three theoretical models (lines), see the legend and main text; (b) Curie temperature dependence on the iron content x (solid symbols) in $Pd_{1-x}Fe_x$ alloy films. Solid blue line is a fit with the Mohn-Schwarz model; and dashed red line is a fit with the Korenblit-Shender-Shklovsky model. Green symbols – experimental $M(x)$.

On cooling, the bubbles of spin-polarized palladium electrons grow in size, and at a temperature when they overlap, the long-range ferromagnetic order sets in. The onset of ferromagnetism thereby occurs through a percolation process involving these spin-polarized bubbles [51]. Korenblit, Shender and Shklovsky (see Ref. [52] and citations therein) have elaborated a model of magnetic ordering for Pd-Fe like alloys with low concentration of ferromagnetism-inducing dopant based on a percolation of magnetically-polarized bubbles. The proposed potential of an indirect exchange interaction between two magnetic atoms has a form:

$$V(r) = V_0(R/r)e^{-r/R} \qquad (3)$$

Here V_0 determines the interaction energy scale, $R = a/\sqrt{1+\Gamma} \gg a$ is an interaction range (a is the interatomic distance), and $(1+\Gamma)^{-1}$ is the static susceptibility enhancement factor of the host [52].

The reduced magnetization σ at a certain temperature T equals to a probability of a magnetic ion occurrence inside the "infinite" magnetic cluster uninterruptedly extending over the entire sample. The resulting $\sigma(T)$ dependence may take the shape of a flattened convex curve for $(4/3)\pi nR^3 \sim 10^{-2} - 10^{-3}$ or even a concave curve for $(4/3)\pi nR^3 < 10^{-4}$ with the threshold depending on the magnetic dopant concentration and the actual range of the interaction provided by the host (n is a number of the dopant atoms per unit volume). The "tail" above T_C cannot be described by this "mean-distance" theory because it does not account for the short-range order effects of the nearest or close neighbors.

The result of the experimental $M_s(T)$ data fit with the Korenblit-Shender-Shklovsky theory is presented in Figure 4a for the sample of $Pd_{1-x}Fe_x$ alloy with $x = 0.011$ (recall that the reduced $\sigma(\tau)$ curves have identical shape for $x = 0.011 - 0.07$). The best-fit parameter R varies from $\simeq$ 130 pm to $\simeq$ 70 pm for iron content within the range from 0.011 to 0.07. These values look unexpectedly small and concentration dependent, the latter has not been inherent to the original theory [52].

Figure 4a presents the fits with the three models mentioned above to the experimental $M_s(T)$ data for the $Pd_{1-x}Fe_x$ alloy film with the iron content $x = 0.011$. All the three models fit the data fairly well; however, a model selection based solely on the best-fit criterion would be misleading because of very different assumptions behind these theories. Additional arguments could be obtained from the concentration dependence of the transition temperature $T_C(x)$.

Concentration dependence of the ferromagnetic transition temperature

Mohn-Schwartz Model

The spin-fluctuation model of itinerant electron paramagnets doped with magnetic impurities was developed by Mohn and Schwartz to calculate the temperature of the ferromagnetic transition in alloys of palladium with elements of the iron group [41,53]. The transition temperature T_C is determined by the divergence point of the magnetic susceptibility, which, in turn, is given by the balance of the inverse susceptibilities of the host and magnetic impurity contributions. The concentration-dependent T_C can be found then as a real-valued solution of the cubic equation,

$$A + 5B\alpha k_B T_C + 35C(\alpha k_B T_C)^2 = \frac{(g-1)^2}{\mu_B^2 n} I^2 \frac{2S(S+1)}{3k_B T_C} \qquad (4)$$

where A, B and C are the expansion coefficients of the Landau theory, α is the proportionality coefficient between the mean square of the fluctuating magnetic moment of the host and temperature (see Ref. [53] and citations therein), g and S are the spectroscopic g-factor and spin of magnetic impurity (iron in our case), and finally, I is the constant of coupling between the localized impurity moment and the itinerant electron spin. Left-hand side of Equation 4 is nothing but the inverse magnetic susceptibility of palladium, the fitting of which to a pure palladium susceptibility data fixes parameters $B\alpha/A$ and $C\alpha^2/A$. Namely, $5B\alpha k_B/A$=172·(35$C(\alpha k_B)^2/A$) K^{-1} from the maximum of Pd susceptibility at $T_{max} \sim 86$ K (Ref. [25], Figure 2.1), and $35C(\alpha k_B)^2/A = 1.4\times10^{-5}$ K^2 from $\chi(T_{max})/\chi(T=0) \approx 1.115$. All poorly determined quantities in the numerator of the r.h.s. (Equation 4) can be absorbed into a single parameter subject to the fitting procedure: (T_C·r.h.s./A) = 2920 K. The fitted curve is shown in **Figure 4b** by the blue solid line. The resulting concentration dependence of the T_C is found non-linear because of the non-monotonous temperature dependence of the palladium magnetic susceptibility with the maximum at $T_{max} \sim 86$ K. Due to this, the concentration dependence $T_C(x)$ gradually switches from higher increment at low iron content x to the reduced increment once the T_C surpasses $\sim$86 K. The dopant content threshold is within 0.03 – 0.045 of iron in palladium (see Figure 4b).

Korenblit-Shender-Shklovsky Model

Korenblit, Shender and Shklovsky suggested an expression for the T_C dependence on x within their model of dilute alloy [52]. The Curie temperature corresponds to a percolation of spin-polarized bubbles and occurrence of the "infinite" magnetic cluster:

$$T_C = V_C \frac{Rn^{1/3}}{0.87} \exp\left(-\frac{0.87}{Rn^{1/3}}\right), \qquad (5)$$

where $V_c \approx V_0 S^2$, and the numerical factor comes from the percolation theory. The direct fitting of Equation (5) to the experimental data (see Figure 4b) allows to determine the pre-factor V_c in Equation (5) as $V_c = 650 \pm 120$ K, and the R value of 470 $\pm$ 40 pm. The $T_C(x)$ dependence is non-linear convex, and this non-linearity is ascribed in Ref. [52] to spatial fluctuations of molecular fields, especially at the lower side of concentrations. The fitting is quite good, however, the

mismatch between $R \sim 100$ pm and $R \sim 470$ pm, determined from the fitting to $M_s(T)$ and $T_C(x)$ data, respectively, looks confusing with no explanation at the moment.

Both models describe the concentration dependence of the magnetic transition temperature quite well. However, the Korenblit-Shender-Shklovsky model requires the effective range of the interaction between the impurity atoms $R >> a$, where a is interatomic distance (see Equation 3 and its description), whereas fitting to our experimental data gives for the R parameter the maximal value of 470 pm which is about two interatomic distances. Moreover, the Korenblit-Shender-Shklovsky model predicts gradual change of the shape of $M_s(T)$-dependence from convex on the high impurity concentration side towards the concave upon dilution. No indication of this trend is visible in our experimental data on $M_s(T)$, Figure 4a. On the other hand, the Mohn-Schwarz spin-fluctuation model does not imply the $M_s(T)$ shape to change until the host susceptibility dominates in the net magnetic response of the alloy. It looks (see the fourth column of Table 1 above) that for our $Pd_{1-x}Fe_x$ samples with $x = 0.011 - 0.062$, the palladium host magnetism dominates over the iron one. So, from our analysis of the particular palladium-rich $Pd_{1-x}Fe_x$ alloy we opt for the spin-fluctuation model, albeit not at the evidence level.

In the spin-fluctuation model, the conduction band exchange splitting, which determines the coherence length of Cooper pairs in the $Pd_{1-x}Fe_x$ [19,20], scales with the concentration dependence of the magnetic moment $M_s(x)$, Figure 2a and Table 1. Once the coherence length is determined for a certain iron content x from the critical current *versus* the alloy thickness dependence (see Figures 2 and 4 of Ref. [18] adapted to the experimental data of Ref. [21] for $x = 0.01$; or Figure 5 and bottom of the page column below in Ref. [23], $x = 0.03$) it can be re-calculated for desired iron content x with the use of $M_s(x)$ (see Table 1 and Figure 4b).

FMR quantification of magnetic anisotropies

The angular dependence of the FMR field for resonance, Figure 3a, was analyzed using the free energy density expansion (see in Reviews [54,55]) assuming the cubic symmetry of the film lattice with small tetragonal distortion [37]:

$$E = -\mathbf{M}\cdot\mathbf{H} + 2\pi M_s^2\alpha_3^2 - K_p\alpha_3^2 - \frac{1}{2}K_1\left(\alpha_1^4 + \alpha_2^4 + \alpha_3^4\right) - \frac{1}{2}K_2\alpha_3^4, \quad (6)$$

where the first term is the Zeeman energy in an external magnetic field; the second term describes the demagnetization energy arising from the thin-film shape of the sample; the third term accumulates the "perpendicular" anisotropy induced by interfaces and a leading term due to the tetragonal lattice distortion; the last two terms are the cubic and second-order tetragonal anisotropy contributions. The indexed α_i's represent the directional cosines of the magnetization vector $\boldsymbol{M}$ with respect to the crystallographic axes ([100], [010], [001]) of the MgO(001) substrate [54,55], and M_s is a saturation magnetization at a given temperature.

The anisotropy constants K_i and spectroscopic g-factor are determined by simultaneous fitting of the in-plane (see Figure 3a) and out-of-plane (not shown here) angular dependencies of the resonance field. Resonance field values were obtained by simultaneous solution of the system of Suhl and equilibrium equations (see general prescriptions in Reviews [54,55] and for the particular case of $Pd_{0.92}Fe_{0.08}$ in Ref. [37]). Upon fitting the FMR data, the saturation magnetization M_s measured by VSM was used to provide the stable convergence of the fitting procedure with the minimal scatter of the freely varied parameters.

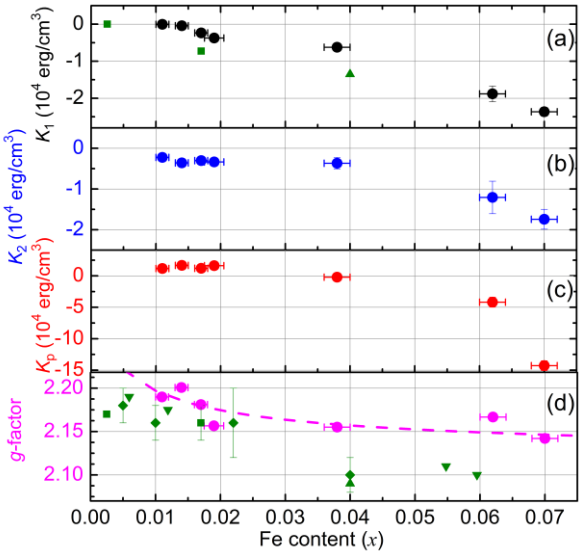

Figure 5 Dependences of the anisotropy constants K_1 (a), K_2 (b) and K_p (c) and of the g-factor (d) are shown by solid circles. Dashed line in (d) presents the fit (see text). Results from other works are presented: for thin film – ▲ [32], for bulk single crystal – ■ [40], for bulk polycrystal – ◆ [56,57], for a thick polycrystalline film – ▼ [59].

Concentration dependences of the anisotropy constants and the spectroscopic g-factor are presented in **Figure 5**. The figure shows that the magnitudes of the cubic, K_1, and the second-order tetragonal, K_2, anisotropy constants change gradually with an increase of the iron content (concentration). The cumulative perpendicular and the first-order tetragonal anisotropy, K_p, first, keeps its positive magnitude nearly independent on the iron content, then it changes sign at $x \sim 0.04$ and increases in accelerating manner in the negative values domain. To distinguish the evolution of the intrinsic anisotropies of $Pd_{1-x}Fe_x$ alloy from that associated with the thin film morphology we compare our FMR results with data found in the literature for the bulk sample and for

various films. Indeed, FMR studies of the bulk and thick-film $Pd_{1-x}Fe_x$ reported on only cubic anisotropy, the energy scale of which, K_1, is in a good agreement with ours (see Figure 5).

The g-factor for our films lies in the range of 2.13 – 2.2 (Fig. 5d). It is a typical value for this material, for example, $g = 2.09 – 2.17$ ($x = 0.025 – 0.06$) [32,40,56-59]. The dependence of the g-factor on the iron content x was fit following the prescription of Ref. [40]. The result is shown by the dashed line in Fig. 5d. The values of the g-factors obtained from the fit are $g_{Pd} = 2.28$ and $g_{Fe} = 2.0$. These quantities are important in the modeling of the magnetic moment switching by spin-polarized current or magnetic field pulses [60].

Hysteresis loops analysis

The FMR field for resonance in all studied films has values larger than 1000 Oe, which significantly exceeds both coercive fields (maximum 23 Oe, see Table 1) and saturation fields (a few hundred Oe, see Figure 3b). Therefore, films under resonance conditions are inevitably in a saturated (single-domain) state. However, among the desired properties of $Pd_{1-x}Fe_x$ thin films, mapped on their application in superconducting spintronics, one finds magnetic uniformity and a possibility of a coherent rotation of the magnetization in the film plane by weak magnetic fields. Such information can be obtained from an analysis of the shape of the hysteresis loops. Our epitaxial films are characterized by a pronounced anisotropy in the film plane (Figure 3a), which is a prerequisite for a coherent (over the film volume) magnetization reversal. The most informative is the shape of the hysteresis loops in the field applied along the hard in-plane direction; representative loops are shown in Figure 3b. It is seen that the shape of the loops is qualitatively identical for the three compositions presented. In addition, left-top and left-bottom insets of Figure 3b demonstrate robustness of the hysteretic and magnetization properties after 6 months at ambient conditions without any protection.

To model the hysteresis loops we have applied a model of the uniform magnetization rotation (Stoner-Wohlfarth mode). Equilibrium orientation of the magnetic moment φ_M was determined by finding a minimum of the free energy, Equation 5, with the magnetic field of a given magnitude applied at a given angle φ_H in the film plane. The anisotropy constant K_1 obtained from the above analysis of the FMR data has been used to model the hysteresis loops. The measured magnetization of the film corresponds to the projection of the equilibrium magnetization on the direction of the applied field [61].

Calculated loops in Figure 3b reproduce well the experimental ones. Successful simulation of the hysteresis loops of thin epitaxial $Pd_{1-x}Fe_x$ films with $x \leq 0.07$ within the Stoner-Wohlfarth model allows us to conclude on predominantly coherent magnetic moment rotation at low temperatures. This, in turn, confirms the promise of these materials for the use as an F-layer in the components of superconducting spintronics.

CONCLUSION

Epitaxial $Pd_{1-x}Fe_x$ ($0.011 \leq x \leq 0.07$) films were grown on the single-crystal MgO (001) substrates, and magnetic properties of the films, being of the key importance for superconducting spintronics, have been extensively studied with the combination of the VSM magnetometry and ferromagnetic resonance spectroscopy. All fundamental magnetic parameters, such as the Curie temperature and saturation magnetization, as well as the magnetic anisotropy constants were determined, and their dependences on the iron content x were obtained for the first time. The shape of the magnetization dependence on temperature was found universal in the studied iron content range. It is extensively discussed in the framework of several models of dilute magnetic alloys, and it was concluded that the spin-fluctuation model has the least controversies with our experimental data. The in-plane magnetic hysteresis loops were successfully reproduced utilizing the FMR data for the magnetic anisotropies and the Stoner-Wohlfarth model of the magnetic moment reversal. This allowed us to conclude on the predominantly coherent magnetic moment switching upon remagnetization at low temperatures. The presented experimental data cover the range $0.011 \leq x \leq 0.07$ of the iron content in $Pd_{1-x}Fe_x$ alloy suitable for different components of cryogenic spintronic and quantum computing circuits based on Josephson π-junctions.

Received xxx 2020; accepted xxx 2020;
Published online xxx 2020

1 Nikonov DE, Young IA. Overview of beyond-CMOS devices and a uniform methodology for their benchmarking. Proc IEEE 2013, 101: 2498-2533
2 Markov IL. Limits on fundamental limits to computation. Nature 2014, 512: 147-154
3 Olofsson A. Silicon compilers – version 2.0 (DARPA). International Symposium on Physical Design, http://www.ispd.cc/slides/2018/k2.pdf, open access: March 25-28, 2018, Monterey CA
4 Xiu L. Time Moore. IEEE Solid-State Circ Mag 2019, 11: 39-55
5 Shalf J. The future of computing beyond Moore's law. Phil Trans R Soc A 2020, 378: 20190061(15)
6 Moore GE. Cramming more components onto integrated circuits. Electronics 1965, 38: 33–35
7 Mukhanov OA. Energy-efficient single flux quantum technology. IEEE Trans Appl Supercond 2011, 21: 760-769
8 Likharev KK. Superconductor digital electronics. Physica C 2012, 482: 6–18
9 Tolpygo SK. Superconductor digital electronics: scalability and energy efficiency issues. Low Temp Phys 2016, 42: 361-379
10 Soloviev II, Klenov NV, Bakurskiy SV, Kupriyanov MYu, Gudkov AL, Sidorenko AS. Beyond Moore's technologies: operation principles of a superconductor alternative. Beilstein J Nanotechnol 2017, 8: 2689–2710
11 Holmes DS, Ripple AL, Manheimer MA. Energy-efficient superconducting computing – power budgets and requirements. IEEE Trans Appl Supercond 2013, 23: 1701610(10)
12 Volkmann MH, Sahu A, Fourie CJ, Mukhanov OA. Implementation

of energy efficient single flux quantum digital circuits with sub-aJ/bit operation. Supercond Sci Technol 2013, 26: 015002(16)
13 Mukhanov OA, Semenov VK, Likharev KK. Ultimate performance of RSFQ logic circuits. IEEE Trans Magn 1987, 23: 759–762
14 Cryogenic Computing Complexity (C3) Program. https://wwwiarpagov/indexphp/research-programs/c3
15 Manheimer MA. Cryogenic Computing Complexity program: phase 1 Introduction. IEEE Trans Appl Supercond 2015, 25: 1301704(4)
16 Larkin TI, Bol'ginov VV, Stolyarov VS, Ryazanov VV, Vernik IV, Tolpygo SK, Mukhanov OA. Ferromagnetic Josephson switching device with high characteristic voltage. Appl Phys Lett 2012, 100: 222601(5)
17 Ryazanov VV, Bol'ginov VV, Sobanin DS, Vernik IV, Tolpygo SK, Kadin AM, Mukhanov OA. Magnetic Josephson junction technology for digital and memory applications. Phys Procedia 2012, 36: 35-41
18 Bakurskiy SV, Klenov NV, Soloviev II, Bol'ginov VV, Ryazanov VV, Vernik IV, Mukhanov OA, Kupriyanov MYu, Golubov AA. Theoretical model of superconducting spintronic SIsFS devices. Appl Phys Lett 2013, 102: 192603(4)
19 Buzdin AI. Proximity effects in superconductor-ferromagnet heterostructures. Rev Mod Phys 2005, 77: 935-976
20 Linder J, Robinson JWA. Superconducting spintronics. Nature Phys 2015, 11: 307-315
21 Vernik IV, Bol'ginov VV, Bakurskiy SV, Golubov AA, Kupriyanov MYu, Ryazanov VV, Mukhanov O. Magnetic Josephson junctions with superconducting interlayer for cryogenic memory. IEEE Trans Appl Supercond 2013, 23:1701208(8)
22 Niedzielski BM, Diesch SG, Gingrich EC, Wang Y, Loloee R, Pratt Jr WP, , Birge NO. Use of Pd–Fe and Ni–Fe–Nb as soft magnetic layers in ferromagnetic Josephson junctions for nonvolatile cryogenic memory. IEEE Trans Appl Supercond 2014, 24: 1800307(7)
23 Glick JA, Loloee R, Pratt Jr WP, Birge NO. Critical current oscillations of Josephson junctions containing PdFe nanomagnets. IEEE Trans Appl Supercond 2017, 27: 1800205(5)
24 Dayton IM, Sage T, Gingrich EC, Loving MG, Ambrose TF, Siwak NP, Keebaugh S, Kirby C, Miller DL, Herr AY, Herr QP, Naaman O. Experimental demonstration of a Josephson magnetic memory cell with a programmable π-junction. IEEE Magn Lett 2018, 9: 3301905(5)
25 Nieuwenhuys GJ. Magnetic behaviour of cobalt, iron and manganese dissolved in palladium. Adv Phys 1975, 24: 515-591
26 Golovchanskiy IA, Bol'ginov VV, Abramov NN, Stolyarov VS, Ben Hamida A, Chichkov VI, Roditchev D, Ryazanov VV. Magnetization dynamics in dilute $Pd_{1-x}Fe_x$ thin films and patterned microstructures considered for superconducting electronics. J Appl Phys 2016, 120: 163902
27 Webb DJ, McKinley JD. Two-dimensional magnetism in Pd (12 at% Fe) films. Phys Rev Lett 1993, 70: 509-511
28 Arham HZ, Khaire TS, Loloee R, Pratt Jr WP, Birge NO. Measurement of spin memory lengths in PdNi and PdFe ferromagnetic alloys. Phys Rev B 2009, 80: 174515(7)
29 Uspenskaya LS, Rakhmanov AL, Dorosinskii LA, Bozhko SI, Stolyarov VS, Bol'ginov VV. Magnetism of ultrathin $Pd_{99}Fe_{01}$ films grown on niobium. Mater Res Expr 2014, 1: 036104(11)
30 Bol'ginov VV, Tikhomirov OA, Uspenskaya LS. Two-component magnetization in $Pd_{99}Fe_{01}$ thin films. JETP Letters 2017, 105: 169-173
31 Schöck M, Sürgers C, Löhneysen v H. Superconducting and magnetic properties of $Nb/Pd_{1-x}Fe_x/Nb$ triple layers. Eur Phys Journ B 2000, 14: 1-10
32 Garifullin IA, Tikhonov DA, Garif'yanov NN, Fattakhov MZ, Theis-Bröhl K, Westerholt K, Zabel H. Possible reconstruction of the ferromagnetic state under the influence of superconductivity in epitaxial $V/Pd_{1-x}Fe_x$ bilayers. Appl Magn Reson 2002, 22: 439-452
33 Salikhov RI, Garif'yanov NN, Garifullin IA, Tagirov LR, Westerholt K, Zabel H. Spin screening effect in superconductor/ferromagnet thin film heterostructures studied using nuclear magnetic resonance. Phys Rev B 2009, 80: 2145231
34 Ewerlin M, Pfau B, Günther CM, Schaffert S, Eisebitt S, Abrudan R, Zabel H. Exploration of magnetic fluctuations in PdFe films. Journ Phys: Cond Matter 2013, 25: 266001
35 Wagner T, Richter G, Rühle M. Epitaxy of Pd thin films on (100) $SrTiO_3$: A three-step growth process. J Appl Phys 2001, 89: 2606-2612
36 Esmaeili A, Yanilkin IV, Gumarov AI, Vakhitov IR, Gabbasov BF, Kiiamov AG, Rogov AM, Osin YuN, Denisov AE, Yusupov RV, Tagirov LR. Epitaxial growth of thin $Pd_{1-x}Fe_x$ films on MgO single crystal. Thin Sol Films 2019, 669: 338-344
37 Esmaeili A, Vakhitov IR, Yanilkin IV, Gumarov AI, Khaliulin BM, Gabbasov BF, Aliyev MN, Yusupov RV, Tagirov LR. FMR studies of ultra-thin epitaxial $Pd_{092}Fe_{008}$ film. Appl Magn Reson 2018, 49: 175–183
38 Crangle J, Goodman GM. The magnetization of pure iron and nickel. Proc R Soc Lond A 1971, 321: 477-491
39 Crangle J, Scott WR. Dilute ferromagnetic alloys. J Appl Phys 1965, 36: 921-928
40 Bagguley DMS, Robertson JA. Resonance and magnetic anisotropy in dilute alloys of Pd, Pt with Fe, Co and Ni. Journ Phys F: Metal Phys 1974, 4: 2282-2296
41 Mohn P. Magnetism in the Solid State. Springer Series in Solid-State Sciences v134, Springer 2006
42 Coey JMD. Magnetism and Magnetic Materials. Cambridge University Press 2010: Ch 5
43 Murata KK, Doniach S. Theory of magnetic fluctuations in itinerant ferromagnets. Phys Rev Lett 1972, 29: 285-288
44 Lonzarich GG, Taillefer L. Effect of spin fluctuations on the magnetic equation of state of ferromagnetic or nearly ferromagnetic metals. J Phys C: Solid State Phys 1985, 18: 4339-4371
45 Wagner D. The fixed-spin-moment method and fluctuations. J Phys: Cond Matt 1989, 1: 4635-4642
46 Kuz'min MD. Landau-type parametrization of the equation of state of a ferromagnet. Phys Rev B 2008, 77: 184431
47 Waske A, Hermann H, Mattern N, Skokov K, Gutfleisch O, Eckert J. Magnetocaloric effect of an Fe-based metallic glass compared to benchmark gadolinium. Journ Appl Phys 2012, 112: 123918(7)
48 Handrich K. A simple model for amorphous and liquid ferromagnets. Phys Stat Sol (b) 1969, 32: K55-K58
49 Kobe S. Spontaneous magnetization of an amorphous ferromagnet. Phys Stat Sol (b) 1970, 41: K13-K15
50 Gallagher KA, Willard MA, Zabenkin VN, Laughlin DE, McHenry ME. Distributed exchange interactions and temperature dependent magnetization in amorphous $Fe_{88-x}Co_xZr_7B_4Cu_1$ alloys. Journ Appl Phys 1999, 85: 5130-5132
51 Ododo JC. Percolation concentration and saturation of the Pd moment in ferromagnetic Pd alloys. Journ Phys F: Metal Phys 1983, 13: 1291-1309
52 Korenblit IYa, Shender EF. Ferromagnetism of disordered systems. Sov Phys - Uspekhi 1978, 21: 832-851
53 Mohn P, Schwarz K. Supercell calculations for transition metal impurities in palladium. J Phys: Cond Matter 1993, 5: 5099-5112
54 Heinrich B, Cochran JF. Ultrathin metallic magnetic films: magnetic anisotropies and exchange interactions. Adv Phys 1993, 42: 523-639
55 Farle M. Ferromagnetic resonance of ultrathin metallic layers. Rep Progr Phys 1998, 61: 755-826
56 Bagguley DMS, Crossley WA, Liesegang J. Ferromagnetic resonance in a series of alloys: II Binary alloys of cobalt with platinum and palladium, and one iron-palladium alloy. Proc Phys Soc 1967, 90: 1047-1058
57 Bagguley DMS, Robertson JA. Ferromagnetic resonance in dilute binary alloys of Pd and Pt with Fe and Co. Phys Lett A 1968, 27: 516-517
58 Miyata N, Tomotsune K, Nakada H, Hagiwara M, Kadomatsu H, Fujiwara H. Ferromagnetic crystalline anisotropy of $Pd_{1-x}Fe_x$ alloys I ($x \lesssim 03$, FCC Phase). Journ Phys Soc Japan 1986, 55: 946-952
59 Hardison DL, Thompson ED. Spin wave resonance on PdFe alloys. Journ Phys Colloq 1971, 32(C1): 565-566
60 Stiles MD, Miltat J. Spin-transfer torque and dynamics. In: Spin dynamics in confined magnetic structures III (ed by Hillebrands B and Thiaville A) Berlin-Heidelberg: Springer-Verlag 2006: 225-308
61 Vonsovskii SV, Hardin ER. Magnetism. New York: Wiley 1974, V2:

635 p

Acknowledgements The support by the RSF grant No. 18-12-00459 is gratefully acknowledged. The authors indebted to V.V. Ryazanov, V.V. Bol'ginov and V.S. Stolyarov (ISSP of RAS, Chernogolovka) for stimulating discussions and introduction to the subject. TEM study had been done using equipment of "Physics and technology of micro- and nanostructures" Center at IPM RAS, Nizhny Novgorod. The magnetic properties were measured utilizing the equipment of the PCR Federal Center of Shared Facilities of Kazan Federal University.

Author contributions Esmaeili A, Yanilkin IV and Gumarov AI designed and engineered the samples; Yanilkin IV and Vakhitov IR performed magnetic measurements, while Gabbasov BF and Yusupov RV carried out FMR measurements; Tatarsky DA has made the sample preparation for and TEM imaging; Yanilkin IV, Yusupov RV and Tagirov LR processed the data and wrote the manuscript. All authors contributed to the general discussion and finalizing of the manuscript.

Conflict of interest The authors declare that they have no conflict of interest.

Igor Yanilkin, graduated from Moscow Institute of Physics and Technology (MIPT, Dolgoprudny) in 2010, received PhD in 2017 from Kazan National Research Technological University (KNRTU, Russia). In 2015 he becomes a Researcher of the Solid State Physics Department at Kazan Federal University (KFU, Russia). Nowadays Dr. I. Yanilkin is Senior Researcher of the research lab "Synthesis and Analysis of Thin-Film Structures" of KFU, his research interests include thin films, magnetic nanostructures, thin-film heterostructures, superconductor/ferromagnet heterostructures.

Roman Yusupov received his PhD in 2000 from Kazan State University (KSU, Russia). In 2005-2008 he was studying various strongly-correlated electron systems by femtosecond laser spectroscopy at Jozef Stefan Institute (Slovenia). Since 2010 he is an Associate Professor and from 2014 the Senior Researcher of the Center for Quantum Technologies at Kazan Federal University. His fields of interest include time-resolved optics and magnetooptics, thin films, frustrated magnetism, inhomogeneous states in quantum paramagnets and paraelectrics.

Lenar Tagirov received PhD in 1981 from Kazan State University (KSU, Russia) and DSc in 1996 from National Research Nuclear University (MEPhI, Moscow). In 2008 he becomes a head of the Solid State Physics Department at KSU. In 2016, he joins Zavoisky Physical-Technical Institute of Kazan Scientific Center of RAS. Prof. L. Tagirov leads the research lab "Synthesis and Analysis of Thin-Film Structures", his research interests include magnetic nanostructures, thin-film heterostructures, superconductor/ferromagnet heterostructures, plasmonic metamaterials.

外延薄膜 $Pd_{1-x}Fe_x$ 合金－用于超导自旋电子学的可调铁磁体李飞, 张力

Aliriza Esmaeili, Igor V. Yanilkin, Amir I. Gumarov, Iskander R. Vakhitov, Bulat F. Gabbasov, Roman V. Yusupov*, Dmitriy A. Tatarsky, Lenar R. Tagirov

合成并广泛研究了外延富钯 $Pd_{1-x}Fe_x$ 合金薄膜，将其作为可调谐铁磁材料用于超导自旋电子学。选择(001)取向的MgO单晶衬底和 x = 0.01-0.07 的组成范围以支持外延生长，并提供具有从磁性非常软的铁磁体(用于存储应用)到中等软和中等硬度的磁性的薄膜。可编程逻辑和电路偏置。通过对磁力分析和铁磁共振数据的分析获得了饱和磁化强度和磁各向异性常数对铁含量x的依赖性。在现有的稀铁磁合金理论框架内讨论了实验结果。 Stoner-Wohlfarth 模型内的磁滞回线的仿真表明，在低温下，主要的相干磁矩旋转。获得的结果汇编了单晶薄膜形式的钯-铁合金的磁性能数据库，该数据库被认为是用于超导自旋电子学的材料。